

Combined Forward-Backward Asymmetry Measurements in Top-Antitop Quark Production at the Tevatron

T. Aaltonen \dagger^{21} V.M. Abazov \ddagger^{13} B. Abbott \ddagger^{115} B.S. Acharya \ddagger^{79} M. Adams \ddagger^{97} T. Adams \ddagger^{96} J.P. Agnew \ddagger^{93} G.D. Alexeev \ddagger^{13} G. Alkhazov \ddagger^{87} A. Alton $\dagger^{kk,31}$ S. Amerio $\dagger^{bbb,39}$ D. Amidei \dagger^{31} A. Anastassov $\dagger^{w,15}$ A. Annovi \dagger^{17} J. Antos \dagger^{12} G. Apollinari \dagger^{15} J.A. Appel \dagger^{15} T. Arisawa \dagger^{51} A. Artikov \dagger^{13} J. Asaadi \dagger^{47} W. Ashmanskas \dagger^{15} A. Askew \ddagger^{96} S. Atkins \ddagger^{105} B. Auerbach \dagger^2 K. Augsten \ddagger^{61} A. Aurisano \dagger^{47} V. Aushev \ddagger^{90} Y. Aushev \ddagger^{90} C. Avila \ddagger^{59} F. Azfar \dagger^{38} F. Badaud \ddagger^{64} W. Badgett \dagger^{15} T. Bae \dagger^{25} L. Bagby \ddagger^{15} B. Baldin \ddagger^{15} D.V. Bandurin \ddagger^{122} S. Banerjee \ddagger^{79} A. Barbaro-Galtieri \dagger^{26} E. Barberis \ddagger^{106} P. Baringer \ddagger^{104} V.E. Barnes \dagger^{43} B.A. Barnett \dagger^{23} P. Barria $\dagger^{ddd,41}$ J.F. Bartlett \ddagger^{15} P. Bartos \dagger^{12} U. Bassler \ddagger^{69} M. Bauce $\dagger^{bbb,39}$ V. Bazterra \ddagger^{97} A. Bean \ddagger^{104} F. Bedeschi \dagger^{41} M. Begalli \ddagger^{56} S. Behari \dagger^{15} L. Bellantoni \ddagger^{15} G. Bellettini $\dagger^{ccc,41}$ J. Bellinger \dagger^{53} D. Benjamin \dagger^{14} A. Beretvas \dagger^{15} S.B. Beri \ddagger^{77} G. Bernardi \ddagger^{68} R. Bernhard \ddagger^{73} I. Bertram \ddagger^{91} M. Besançon \ddagger^{69} R. Beuselinck \ddagger^{92} P.C. Bhat \ddagger^{15} S. Bhatia \ddagger^{107} V. Bhatnagar \ddagger^{77} A. Bhatti \dagger^{45} K.R. Bland \dagger^5 G. Blazey \ddagger^{98} S. Blessing \ddagger^{96} K. Bloom \ddagger^{108} B. Blumenfeld \dagger^{23} A. Bocci \dagger^{14} A. Bodek \dagger^{44} A. Boehlein \ddagger^{15} D. Boline \ddagger^{112} E.E. Boos \ddagger^{85} G. Borissov \ddagger^{91} D. Bortoletto \dagger^{43} M. Borysova $\dagger^{vv,90}$ J. Boudreau \dagger^{42} A. Boveia \dagger^{11} A. Brandt \ddagger^{119} O. Brandt \ddagger^{74} L. Brigliadori $\dagger^{aaa,6}$ M. Brochmann \ddagger^{123} R. Brock \ddagger^{32} C. Bromberg \dagger^{32} A. Bross \ddagger^{15} D. Brown \ddagger^{68} E. Brucken \dagger^{21} X.B. Bu \ddagger^{15} J. Budagov \dagger^{13} H.S. Budd \dagger^{44} M. Buehler \ddagger^{15} V. Buescher \ddagger^{75} V. Bunichev \ddagger^{85} S. Burdin $\ddagger^{ll,91}$ K. Burkett \dagger^{15} G. Busetto $\dagger^{bbb,39}$ P. Bussey \dagger^{19} C.P. Buszello \ddagger^{89} P. Butti $\dagger^{ccc,41}$ A. Buzatu \dagger^{19} A. Calamba \dagger^{10} E. Camacho-Pérez \ddagger^{82} S. Camarda \dagger^4 M. Campanelli \dagger^{28} F. Canelli $\dagger^{ee,11}$ B. Carls \dagger^{22} D. Carlsmith \dagger^{53} R. Carosi \dagger^{41} S. Carrillo $\dagger^{ll,16}$ B. Casal $\dagger^{jj,9}$ M. Casarsa \dagger^{48} B.C.K. Casey \ddagger^{15} H. Castilla-Valdez \ddagger^{82} A. Castro $\dagger^{aaa,6}$ P. Catastini \dagger^{20} S. Caughron \ddagger^{32} D. Cauz $\dagger^{iiijj,48}$ V. Cavaliere \dagger^{22} A. Cerri $\dagger^{e,26}$ L. Cerrito $\dagger^{rr,28}$ S. Chakrabarti \ddagger^{112} K.M. Chan \ddagger^{102} A. Chandra \dagger^{121} A. Chapelain \ddagger^{69} E. Chapon \ddagger^{69} G. Chen \dagger^{104} Y.C. Chen \dagger^{1} M. Chertok \dagger^{7} G. Chiarelli \dagger^{41} G. Chlachidze \dagger^{15} K. Cho \dagger^{25} S.W. Cho \ddagger^{81} S. Choi \ddagger^{81} D. Chokheli \dagger^{13} B. Choudhary \ddagger^{78} S. Cihangir $\ddagger^{15,*}$ D. Claes \ddagger^{108} A. Clark \dagger^{18} C. Clarke \dagger^{52} J. Clutter \dagger^{104} M.E. Convery \dagger^{15} J. Conway \dagger^{7} M. Cooke $\dagger^{uu,15}$ W.E. Cooper \ddagger^{15} M. Corbo $\dagger^{zz,15}$ M. Corcoran $\ddagger^{121,*}$ M. Cordelli \dagger^{17} F. Couderc \ddagger^{69} M.-C. Cousinou \ddagger^{66} C.A. Cox \dagger^{7} D.J. Cox \dagger^{7} M. Cremonesi \dagger^{41} D. Cruz \dagger^{47} J. Cuevas $\dagger^{yy,9}$ R. Culbertson \dagger^{15} J. Cuth \ddagger^{75} D. Cutts \ddagger^{118} A. Das \ddagger^{120} N. d'Ascenzo $\dagger^{vv,15}$ M. Datta $\dagger^{hh,15}$ G. Davies \ddagger^{92} P. de Barbaro \dagger^{44} S.J. de Jong $\ddagger^{83,84}$ E. De La Cruz-Burelo \ddagger^{82} F. Déliot \ddagger^{69} R. Demina \ddagger^{44} L. Demortier \dagger^{45} M. Deninno \dagger^6 D. Denisov \ddagger^{15} S.P. Denisov \ddagger^{86} M. D'Errico $\dagger^{bbb,39}$ S. Desai \ddagger^{15} C. Deterre $\dagger^{mm,93}$ K. DeVaughan \ddagger^{108} F. Devoto \dagger^{21} A. Di Canto $\dagger^{ccc,41}$ B. Di Ruzza $\dagger^{pp,15}$ H.T. Diehl \ddagger^{15} M. Diesburg \ddagger^{15} P.F. Ding \ddagger^{93} J.R. Dittmann \dagger^5 A. Dominguez \ddagger^{108} S. Donati $\dagger^{ccc,41}$ M. D'Onofrio \dagger^{27} M. Dorigo $\dagger^{kkk,48}$ A. Driutti $\dagger^{iiijj,48}$ A. Drutskoy \ddagger^{33} A. Dubey \ddagger^{78} L.V. Dudko \ddagger^{85} A. Duperrin \ddagger^{66} S. Dutt \ddagger^{77} M. Eads \ddagger^{98} K. Ebina \dagger^{51} R. Edgar \dagger^{31} D. Edmunds \ddagger^{32} A. Elagin \dagger^{11} J. Ellison \ddagger^{95} V.D. Elvira \ddagger^{15} Y. Enari \ddagger^{68} R. Erbacher \dagger^7 S. Errede \dagger^{22} B. Esham \dagger^{22} H. Evans \ddagger^{100} A. Evdokimov \ddagger^{97} V.N. Evdokimov \ddagger^{86} S. Farrington \dagger^{38} A. Fauré \ddagger^{69} L. Feng \ddagger^{98} T. Ferbel \ddagger^{44} J.P. Fernández Ramos \dagger^{29} F. Fiedler \ddagger^{75} R. Field \dagger^{16} F. Filthaut $\ddagger^{83,84}$ W. Fisher \ddagger^{32} H.E. Fisk \ddagger^{15} G. Flanagan $\ddagger^{tt,15}$ R. Forrest \dagger^7 M. Fortner \ddagger^{98} H. Fox \ddagger^{91} J. Franc \ddagger^{61} M. Franklin \dagger^{20} J.C. Freeman \dagger^{15} H. Frisch \dagger^{11} S. Fuess \ddagger^{15} Y. Funakoshi \dagger^{51} C. Galloni $\dagger^{ccc,41}$ P.H. Garbincius \ddagger^{15} A. Garcia-Bellido \ddagger^{44} J.A. García-González \ddagger^{82} A.F. Garfinkel \dagger^{43} P. Garosi $\dagger^{ddd,41}$ V. Gavrilov \ddagger^{33} W. Geng $\ddagger^{66,32}$ C.E. Gerber \ddagger^{97} H. Gerberich \dagger^{22} E. Gerchtein \dagger^{15} Y. Gershtein \ddagger^{109} S. Giagu \dagger^{46} V. Giakoumopoulou \dagger^3 K. Gibson \dagger^{42} C.M. Ginsburg \dagger^{15} G. Ginther \ddagger^{15} N. Giokaris $\dagger^{3,*}$ P. Giromini \dagger^{17} V. Glagolev \dagger^{13} D. Glenzinski \dagger^{15} O. Gogota \ddagger^{90} M. Gold \dagger^{34} D. Goldin \dagger^{47} A. Golossanov \dagger^{15} G. Golovanov \ddagger^{13} G. Gomez \dagger^9 G. Gomez-Ceballos \dagger^{30} M. Goncharov \dagger^{30} O. González López \dagger^{29} I. Gorelov \dagger^{34} A.T. Goshaw \dagger^{14} K. Goulian \dagger^{45} E. Gramellini \dagger^6 P.D. Grannis \ddagger^{112} S. Greder \ddagger^{70} H. Greenlee \ddagger^{15} G. Grenier \ddagger^{71} Ph. Gris \ddagger^{64} J.-F. Grivaz \ddagger^{67} A. Grohsjean $\dagger^{mm,69}$ C. Grossi-Pilcher \ddagger^{11} S. Grünendahl \ddagger^{15} M.W. Grünwald \ddagger^{80} T. Guillemin \ddagger^{67} J. Guimaraes da Costa \dagger^{20} G. Gutierrez \ddagger^{15} P. Gutierrez \ddagger^{115} S.R. Hahn \dagger^{15} J. Haley \ddagger^{116} J.Y. Han \dagger^{44} L. Han \ddagger^{58} F. Happacher \dagger^{17} K. Hara \dagger^{49} K. Harder

†, 93 M. Hare †, 50 A. Harel †, 44 R.F. Harr †, 52 T. Harrington-Taber †^m, 15 K. Hatakeyama †, 5 J.M. Hauptman †, 103
 C. Hays †, 38 J. Hays †, 92 T. Head †, 93 T. Hebbeker †, 72 D. Hedin †, 98 H. Hegab †, 116 J. Heinrich †, 40 A.P. Heinson
 †, 95 U. Heintz †, 118 C. Hensel †, 55 I. Heredia-De La Cruz †ⁿⁿ, 82 M. Herndon †, 53 K. Herner †, 15 G. Hesketh †^{pp}, 93
 M.D. Hildreth †, 102 R. Hirosky †, 122 T. Hoang †, 96 J.D. Hobbs †, 112 A. Hocker †, 15 B. Hoeneisen †, 63 J. Hogan †, 121
 M. Hohlfeld †, 75 J.L. Holzbauer †, 107 Z. Hong †^w, 47 W. Hopkins †^f, 15 S. Hou †, 1 I. Howley †, 119 Z. Hubacek †, 61, 69
 R.E. Hughes †, 35 U. Husemann †, 54 M. Hussein †^{cc}, 32 J. Huston †, 32 V. Hynek †, 61 I. Iashvili †, 111 Y. Ilchenko †, 120
 R. Illingworth †, 15 G. Introzzi †^{ffffggg}, 41 M. Iori †^{hhh}, 46 A.S. Ito †, 15 A. Ivanov †^o, 7 S. Jabeen †^{ww}, 15 M. Jaffré †, 67
 E. James †, 15 D. Jang †, 10 A. Jayasinghe †, 115 B. Jayatilaka †, 15 E.J. Jeon †, 25 M.S. Jeong †, 81 R. Jesik †, 92 P. Jiang
 †, 58, * S. Jindariani †, 15 K. Johns †, 94 E. Johnson †, 32 M. Johnson †, 15 A. Jonckheere †, 15 M. Jones †, 43 P. Jonsson
 †, 92 K.K. Joo †, 25 J. Joshi †, 95 S.Y. Jun †, 10 A.W. Jung †^{yy}, 15 T.R. Junk †, 15 A. Juste †, 88 E. Kajfasz †, 66
 M. Kambeitz †, 24 T. Kamon †, 25, 47 P.E. Karchin †, 52 D. Karmanov †, 85 A. Kasmi †, 5 Y. Kato †ⁿ, 37 I. Katsanos †, 108
 M. Kaur †, 77 R. Kehoe †, 120 S. Kermiche †, 66 W. Ketchum †ⁱⁱ, 11 J. Keung †, 40 N. Khalatyān †, 15 A. Khanov †, 116
 A. Kharchilava †, 111 Y.N. Kharzheev †, 13 B. Kilminster †^{ee}, 15 D.H. Kim †, 25 H.S. Kim †^{bb}, 15 J.E. Kim †, 25 M.J. Kim
 †, 17 S.H. Kim †, 49 S.B. Kim †, 25 Y.J. Kim †, 25 Y.K. Kim †, 11 N. Kimura †, 51 M. Kirby †, 15 I. Kiselevich †, 33
 J.M. Kohli †, 77 K. Kondo †, 51, * D.J. Kong †, 25 J. Konigsberg †, 16 A.V. Kotwal †, 14 A.V. Kozelov †, 86 J. Kraus †, 107
 M. Kreps †, 24 J. Kroll †, 40 M. Kruse †, 14 T. Kuhr †, 24 A. Kumar †, 111 A. Kupco †, 62 M. Kurata †, 49 T. Kurča †, 71
 V.A. Kuzmin †, 85 A.T. Laasanen †, 43 S. Lammel †, 15 S. Lammers †, 100 M. Lancaster †, 28 K. Lannon †^x, 35 G. Latino
 †^{ddd}, 41 P. Lebrun †, 71 H.S. Lee †, 81 H.S. Lee †, 25 J.S. Lee †, 25 S.W. Lee †, 103 W.M. Lee †, 15 X. Lei †, 94 J. Lellouch
 †, 68 S. Leo †, 22 S. Leone †, 41 J.D. Lewis †, 15 D. Li †, 68 H. Li †, 122 L. Li †, 95 Q.Z. Li †, 15 J.K. Lim †, 81 A. Limosani
 †^s, 14 D. Lincoln †, 15 J. Linnemann †, 32 V.V. Lipaev †, 86, * E. Lipeles †, 40 R. Lipton †, 15 A. Lister †^a, 18 H. Liu †, 120
 Q. Liu †, 43 T. Liu †, 15 Y. Liu †, 58 A. Lobodenko †, 87 S. Lockwitz †, 54 A. Loginov †, 54 M. Lokajicek †, 62
 R. Lopes de Sa †, 15 D. Lucchesi †^{bbb}, 39 A. Lucà †, 17, 15 J. Lueck †, 24 P. Lujan †, 26 P. Lukens †, 15 R. Luna-Garcia
 †^{qq}, 82 G. Lungu †, 45 A.L. Lyon †, 15 J. Lys †, 26, * R. Lysak †^d, 12 A.K.A. Maciel †, 55 R. Madar †, 73 R. Madrak
 †, 15 P. Maestro †^{ddd}, 41 R. Magaña-Villalba †, 82 S. Malik †, 45 S. Malik †, 108 V.L. Malyshev †, 13 G. Manca
 †^b, 27 A. Manousakis-Katsikakis †, 3 J. Mansour †, 74 L. Marchese †^{jj}, 6 F. Margaroli †, 46 P. Marino †^{eee}, 41
 J. Martínez-Ortega †, 82 K. Matera †, 22 M.E. Mattson †, 52 A. Mazzacane †, 15 P. Mazzanti †, 6 R. McCarthy †, 112
 C.L. McGivern †, 93 R. McNulty †, 27 A. Mehta †, 27 P. Mehtala †, 21 M.M. Meijer †, 83, 84 A. Melnitchouk †, 15
 D. Menezes †, 98 P.G. Mercadante †, 57 M. Merkin †, 85 C. Mesropian †, 45 A. Meyer †, 72 J. Meyer †^{ss}, 74 T. Miao †, 15
 F. Micconi †, 70 D. Mietlicki †, 31 A. Mitra †, 1 H. Miyake †, 49 S. Moed †, 15 N. Moggi †, 6 N.K. Mondal †, 79 C.S. Moon
 †^z, 15 R. Moore †^{ffff}, 15 M.J. Morello †^{eee}, 41 A. Mukherjee †, 15 M. Mulhearn †, 122 Th. Muller †, 24 P. Murat †, 15
 M. Mussini †^{aaa}, 6 J. Nachtman †^m, 15 Y. Nagai †, 49 J. Naganoma †, 51 E. Nagy †, 66 I. Nakano †, 36 A. Napier †, 50
 M. Narain †, 118 R. Nayyar †, 94 H.A. Neal †, 31 J.P. Negret †, 59 J. Nett †, 47 P. Neustroev †, 87 H.T. Nguyen †, 122
 T. Nigmanov †, 42 L. Nodulman †, 2 S.Y. Noh †, 25 O. Norniella †, 22 T. Nunnemann †, 76 L. Oakes †, 38 S.H. Oh †, 14
 Y.D. Oh †, 25 T. Okusawa †, 37 R. Orava †, 21 J. Orduna †, 118 L. Ortolan †, 4 N. Osman †, 66 C. Pagliarone †, 48 A. Pal
 †, 119 E. Palencia †^e, 9 P. Palni †, 34 V. Papadimitriou †, 15 N. Parashar †, 101 V. Parihar †, 118 S.K. Park †, 81 W. Parker
 †, 53 R. Partridge †^{oo}, 118 N. Parua †, 100 A. Patwa †^{tt}, 113 G. Paulette †^{iiiijjj}, 48 M. Paulini †, 10 C. Paus †, 30 B. Penning
 †, 92 M. Perfilov †, 85 Y. Peters †, 93 K. Petridis †, 93 G. Petrillo †, 44 P. Pétronoff †, 67 T.J. Phillips †, 14 G. Piacentino †^q, 15
 E. Pianori †, 40 J. Pilot †, 7 K. Pitts †, 22 C. Plager †, 8 M.-A. Pleier †, 113 V.M. Podstavkov †, 15 L. Pondrom †, 53
 A.V. Popov †, 86 S. Poprocki †^f, 15 K. Potamianos †, 26 A. Pranko †, 26 M. Prewitt †, 121 D. Price †, 93 N. Prokopenko
 †, 86 F. Prokoshin †^{aa}, 13 F. Ptahos †^g, 17 G. Punzi †^{cc}, 41 J. Qian †, 31 A. Quadt †, 74 B. Quinn †, 107 P.N. Ratoff †, 91
 I. Razumov †, 86 I. Redondo Fernández †, 29 P. Renton †, 38 M. Rescigno †, 46 F. Rimondi †, 6, * I. Ripp-Baudot †, 70
 L. Ristori †, 41, 15 F. Rizatdinova †, 116 A. Robson †, 19 T. Rodriguez †, 40 S. Rolli †^h, 50 M. Rominsky †, 15 M. Ronzani
 †^{ccc}, 41 R. Roser †, 15 J.L. Rosner †, 11 A. Ross †, 91 C. Royon †, 62 P. Rubinov †, 15 R. Ruchti †, 102 F. Ruffini †^{ddd}, 41
 A. Ruiz †, 9 J. Russ †, 10 V. Rusu †, 15 G. Sajot †, 65 W.K. Sakamoto †, 44 Y. Sakurai †, 51 A. Sánchez-Hernández †, 82
 M.P. Sanders †, 76 L. Santi †^{iiiijjj}, 48 A.S. Santos †^{rrr}, 55 K. Sato †, 49 G. Savage †, 15 V. Saveliev †^v, 15 M. Savitskyi †, 90
 A. Savoy-Navarro †^z, 15 L. Sawyer †, 105 T. Scanlon †, 92 R.D. Schamberger †, 112 Y. Scheglov †, 87 H. Schellman
 †, 117, 99 P. Schlabach †, 15 E.E. Schmidt †, 15 M. Schott †, 75 C. Schwanenberger †, 93 T. Schwarz †, 31 R. Schwienhorst
 †, 32 L. Scodellaro †, 9 F. Scuri †, 41 S. Seidel †, 34 Y. Seiya †, 37 J. Sekaric †, 104 A. Semenov †, 13 H. Severini †, 115
 F. Sforza †^{ccc}, 41 E. Shabalina †, 74 S.Z. Shalhout †, 7 V. Shary †, 69 S. Shaw †, 93 A.A. Shchukin †, 86 T. Shears †, 27
 P.F. Shepard †, 42 M. Shimojima †^u, 49 O. Shkola †, 90 M. Shochet †, 11 I. Shreyber-Tecker †, 33 V. Simak †, 61
 A. Simonenko †, 13 P. Skubic †, 115 P. Slattery †, 44 K. Sliwa †, 50 J.R. Smith †, 7 F.D. Snider †, 15 G.R. Snow †, 108

J. Snow \dagger^{114} S. Snyder \dagger^{113} S. Söldner-Rembold \dagger^{93} H. Song \dagger^{42} L. Sonnenschein \dagger^{72} V. Sorin \dagger^4 K. Soustruznik \dagger^{60} R. St. Denis \dagger^{19} , * M. Stancari \dagger^{15} J. Stark \dagger^{65} N. Stefaniuk \dagger^{90} D. Stentz $\dagger^{w,15}$ D.A. Stoyanova \dagger^{86} M. Strauss \dagger^{115} J. Strologas \dagger^{34} Y. Sudo \dagger^{49} A. Sukhanov \dagger^{15} I. Suslov \dagger^{13} L. Suter \dagger^{93} P. Svoisky \dagger^{122} K. Takemasa \dagger^{49} Y. Takeuchi \dagger^{49} J. Tang \dagger^{11} M. Tecchio \dagger^{31} P.K. Teng \dagger^1 J. Thom $\dagger^{f,15}$ E. Thomson \dagger^{40} V. Thukral \dagger^{47} M. Titov \dagger^{69} D. Toback \dagger^{47} S. Tokar \dagger^{12} V.V. Tokmenin \dagger^{13} K. Tollefson \dagger^{32} T. Tomura \dagger^{49} D. Tonelli $\dagger^{e,15}$ S. Torre \dagger^{17} D. Torretta \dagger^{15} P. Totaro \dagger^{39} M. Trovato $\dagger^{eee,41}$ Y.-T. Tsai \dagger^{44} D. Tsybychev \dagger^{112} B. Tuchming \dagger^{69} C. Tully \dagger^{110} F. Ukegawa \dagger^{49} S. Uozumi \dagger^{25} L. Uvarov \dagger^{87} S. Uvarov \dagger^{87} S. Uzunyan \dagger^{98} R. Van Kooten \dagger^{100} W.M. van Leeuwen \dagger^{83} N. Varelas \dagger^{97} E.W. Varnes \dagger^{94} I.A. Vasilyev \dagger^{86} F. Vázquez $\dagger^{l,16}$ G. Velev \dagger^{15} C. Vellidis \dagger^{15} A.Y. Verkheev \dagger^{13} C. Vernieri $\dagger^{eee,41}$ L.S. Vertogradov \dagger^{13} M. Verzocchi \dagger^{15} M. Vesterinen \dagger^{93} M. Vidal \dagger^{43} D. Vilanova \dagger^{69} R. Vilar \dagger^9 J. Vizán $\dagger^{dd,9}$ M. Vogel \dagger^{34} P. Vokac \dagger^{61} G. Volpi \dagger^{17} P. Wagner \dagger^{40} H.D. Wahl \dagger^{96} R. Wallny $\dagger^{j,15}$ M.H.L.S. Wang \dagger^{15} S.M. Wang \dagger^1 J. Warchol \dagger^{102} D. Waters \dagger^{28} G. Watts \dagger^{123} M. Wayne \dagger^{102} J. Weichert \dagger^{75} L. Welty-Rieger \dagger^{99} W.C. Wester III \dagger^{15} D. Whiteson $\dagger^{c,40}$ A.B. Wicklund \dagger^2 S. Wilbur \dagger^7 H.H. Williams \dagger^{40} M.R.J. Williams $\dagger^{xx,100}$ G.W. Wilson \dagger^{104} J.S. Wilson \dagger^{31} P. Wilson \dagger^{15} B.L. Winer \dagger^{35} P. Wittich $\dagger^{f,15}$ M. Wobisch \dagger^{105} S. Wolbers \dagger^{15} H. Wolfmeister \dagger^{35} D.R. Wood \dagger^{106} T. Wright \dagger^{31} X. Wu \dagger^{18} Z. Wu \dagger^5 T.R. Wyatt \dagger^{93} Y. Xie \dagger^{15} R. Yamada \dagger^{15} K. Yamamoto \dagger^{37} D. Yamato \dagger^{37} S. Yang \dagger^{58} T. Yang \dagger^{15} U.K. Yang \dagger^{25} Y.C. Yang \dagger^{25} W.-M. Yao \dagger^{26} T. Yasuda \dagger^{15} Y.A. Yatsunenko \dagger^{13} W. Ye \dagger^{112} Z. Ye \dagger^{15} G.P. Yeh \dagger^{15} K. Yi $\dagger^{m,15}$ H. Yin \dagger^{15} K. Yip \dagger^{113} J. Yoh \dagger^{15} K. Yorita \dagger^{51} T. Yoshida $\dagger^{k,37}$ S.W. Youn \dagger^{15} G.B. Yu \dagger^{14} I. Yu \dagger^{25} J.M. Yu \dagger^{31} A.M. Zanetti \dagger^{48} Y. Zeng \dagger^{14} J. Zennamo \dagger^{111} T.G. Zhao \dagger^{93} B. Zhou \dagger^{31} C. Zhou \dagger^{14} J. Zhu \dagger^{31} M. Zielinski \dagger^{44} D. Ziemska \dagger^{100} L. Zivkovic $\dagger^{zz,68}$ and S. Zucchelli $\dagger^{aaa,6}$

(CDF Collaboration) \dagger

(D0 Collaboration) \ddagger

¹*Institute of Physics, Academia Sinica, Taipei, Taiwan 11529, Republic of China*

²*Argonne National Laboratory, Argonne, Illinois 60439, USA*

³*University of Athens, 157 71 Athens, Greece*

⁴*Institut de Fisica d'Altes Energies, ICREA, Universitat Autònoma de Barcelona, E-08193, Bellaterra (Barcelona), Spain*

⁵*Baylor University, Waco, Texas 76798, USA*

⁶*Istituto Nazionale di Fisica Nucleare Bologna, ^{aaa}University of Bologna, I-40127 Bologna, Italy*

⁷*University of California, Davis, Davis, California 95616, USA*

⁸*University of California, Los Angeles, Los Angeles, California 90024, USA*

⁹*Instituto de Fisica de Cantabria, CSIC-University of Cantabria, 39005 Santander, Spain*

¹⁰*Carnegie Mellon University, Pittsburgh, Pennsylvania 15213, USA*

¹¹*Enrico Fermi Institute, University of Chicago, Chicago, Illinois 60637, USA*

¹²*Comenius University, 842 48 Bratislava, Slovakia; Institute of Experimental Physics, 040 01 Kosice, Slovakia*

¹³*Joint Institute for Nuclear Research, RU-141980 Dubna, Russia*

¹⁴*Duke University, Durham, North Carolina 27708, USA*

¹⁵*Fermi National Accelerator Laboratory, Batavia, Illinois 60510, USA*

¹⁶*University of Florida, Gainesville, Florida 32611, USA*

¹⁷*Laboratori Nazionali di Frascati, Istituto Nazionale di Fisica Nucleare, I-00044 Frascati, Italy*

¹⁸*University of Geneva, CH-1211 Geneva 4, Switzerland*

¹⁹*Glasgow University, Glasgow G12 8QQ, United Kingdom*

²⁰*Harvard University, Cambridge, Massachusetts 02138, USA*

²¹*Division of High Energy Physics, Department of Physics, University of Helsinki, FIN-00014, Helsinki, Finland*

²²*University of Illinois, Urbana, Illinois 61801, USA*

²³*The Johns Hopkins University, Baltimore, Maryland 21218, USA*

²⁴*Institut für Experimentelle Kernphysik, Karlsruhe Institute of Technology, D-76131 Karlsruhe, Germany*

²⁵*Center for High Energy Physics: Kyungpook National University,*

Daegu 702-701, Korea; Seoul National University, Seoul 151-742,

Korea; Sungkyunkwan University, Suwon 440-746,

Korea; Korea Institute of Science and Technology Information,

Daejeon 305-806, Korea; Chonnam National University,

Gwangju 500-757, Korea; Chonbuk National University, Jeonju 561-756,

Korea; Ewha Womans University, Seoul, 120-750, Korea

²⁶*Ernest Orlando Lawrence Berkeley National Laboratory, Berkeley, California 94720, USA*

²⁷*University of Liverpool, Liverpool L69 7ZE, United Kingdom*

²⁸*University College London, London WC1E 6BT, United Kingdom*

²⁹*Centro de Investigaciones Energeticas Medioambientales y Tecnologicas, E-28040 Madrid, Spain*

³⁰*Massachusetts Institute of Technology, Cambridge, Massachusetts 02139, USA*

- ³¹University of Michigan, Ann Arbor, Michigan 48109, USA
³²Michigan State University, East Lansing, Michigan 48824, USA
³³Institute for Theoretical and Experimental Physics, ITEP, Moscow 117259, Russia
³⁴University of New Mexico, Albuquerque, New Mexico 87131, USA
³⁵The Ohio State University, Columbus, Ohio 43210, USA
³⁶Okayama University, Okayama 700-8530, Japan
³⁷Osaka City University, Osaka 558-8585, Japan
³⁸University of Oxford, Oxford OX1 3RH, United Kingdom
³⁹Istituto Nazionale di Fisica Nucleare, Sezione di Padova, ^{bbb}University of Padova, I-35131 Padova, Italy
⁴⁰University of Pennsylvania, Philadelphia, Pennsylvania 19104, USA
⁴¹Istituto Nazionale di Fisica Nucleare Pisa, ^{ccc}University of Pisa,
^{ddd}University of Siena, ^{eee}Scuola Normale Superiore,
^{I-56127 Pisa, Italy,} ^{fff}INFN Pavia, I-27100 Pavia,
^{Italy,} ^{ggg}University of Pavia, I-27100 Pavia, Italy
⁴²University of Pittsburgh, Pittsburgh, Pennsylvania 15260, USA
⁴³Purdue University, West Lafayette, Indiana 47907, USA
⁴⁴University of Rochester, Rochester, New York 14627, USA
⁴⁵The Rockefeller University, New York, New York 10065, USA
⁴⁶Istituto Nazionale di Fisica Nucleare, Sezione di Roma 1,
^{hhh}Sapienza Università di Roma, I-00185 Roma, Italy
⁴⁷Mitchell Institute for Fundamental Physics and Astronomy,
^{Texas A&M University, College Station, Texas 77843, USA}
⁴⁸Istituto Nazionale di Fisica Nucleare Trieste, ⁱⁱⁱGruppo Collegato di Udine,
^{jjj}University of Udine, I-33100 Udine, Italy, ^{kkk}University of Trieste, I-34127 Trieste, Italy
⁴⁹University of Tsukuba, Tsukuba, Ibaraki 305, Japan
⁵⁰Tufts University, Medford, Massachusetts 02155, USA
⁵¹Waseda University, Tokyo 169, Japan
⁵²Wayne State University, Detroit, Michigan 48201, USA
⁵³University of Wisconsin-Madison, Madison, Wisconsin 53706, USA
⁵⁴Yale University, New Haven, Connecticut 06520, USA
⁵⁵LAFEX, Centro Brasileiro de Pesquisas Físicas, Rio de Janeiro, RJ 22290, Brazil
⁵⁶Universidade do Estado do Rio de Janeiro, Rio de Janeiro, RJ 20550, Brazil
⁵⁷Universidade Federal do ABC, Santo André, SP 09210, Brazil
⁵⁸University of Science and Technology of China, Hefei 230026, People's Republic of China
⁵⁹Universidad de los Andes, Bogotá, 111711, Colombia
⁶⁰Charles University, Faculty of Mathematics and Physics,
^{Center for Particle Physics, 116 36 Prague 1, Czech Republic}
⁶¹Czech Technical University in Prague, 116 36 Prague 6, Czech Republic
⁶²Institute of Physics, Academy of Sciences of the Czech Republic, 182 21 Prague, Czech Republic
⁶³Universidad San Francisco de Quito, Quito 170157, Ecuador
⁶⁴LPC, Université Blaise Pascal, CNRS/IN2P3, Clermont, F-63178 Aubière Cedex, France
⁶⁵LPSC, Université Joseph Fourier Grenoble 1, CNRS/IN2P3,
^{Institut National Polytechnique de Grenoble, F-38026 Grenoble Cedex, France}
⁶⁶CPPM, Aix-Marseille Université, CNRS/IN2P3, F-13288 Marseille Cedex 09, France
⁶⁷LAL, Univ. Paris-Sud, CNRS/IN2P3, Université Paris-Saclay, F-91898 Orsay Cedex, France
⁶⁸LPNHE, Universités Paris VI and VII, CNRS/IN2P3, F-75005 Paris, France
⁶⁹CEA Saclay, Irfu, SPP, F-91191 Gif-Sur-Yvette Cedex, France
⁷⁰IPHC, Université de Strasbourg, CNRS/IN2P3, F-67037 Strasbourg, France
⁷¹IPNL, Université Lyon 1, CNRS/IN2P3, F-69622 Villeurbanne Cedex,
^{France and Université de Lyon, F-69361 Lyon CEDEX 07, France}
⁷²III. Physikalisches Institut A, RWTH Aachen University, 52056 Aachen, Germany
⁷³Physikalisches Institut, Universität Freiburg, 79085 Freiburg, Germany
⁷⁴II. Physikalisches Institut, Georg-August-Universität Göttingen, 37073 Göttingen, Germany
⁷⁵Institut für Physik, Universität Mainz, 55099 Mainz, Germany
⁷⁶Ludwig-Maximilians-Universität München, 80539 München, Germany
⁷⁷Panjab University, Chandigarh 160014, India
⁷⁸Delhi University, Delhi-110 007, India
⁷⁹Tata Institute of Fundamental Research, Mumbai-400 005, India
⁸⁰University College Dublin, Dublin 4, Ireland
⁸¹Korea Detector Laboratory, Korea University, Seoul, 02841, Korea
⁸²CINVESTAV, Mexico City 07360, Mexico
⁸³Nikhef, Science Park, 1098 XG Amsterdam, the Netherlands
⁸⁴Radboud University Nijmegen, 6525 AJ Nijmegen, the Netherlands
⁸⁵Moscow State University, Moscow 119991, Russia

- ⁸⁶*Institute for High Energy Physics, Protvino, Moscow region 142281, Russia*
⁸⁷*Petersburg Nuclear Physics Institute, St. Petersburg 188300, Russia*
⁸⁸*Institució Catalana de Recerca i Estudis Avançats (ICREA) and Institut de Física d'Altes Energies (IFAE), 08193 Bellaterra (Barcelona), Spain*
⁸⁹*Uppsala University, 751 05 Uppsala, Sweden*
⁹⁰*Taras Shevchenko National University of Kyiv, Kiev, 01601, Ukraine*
⁹¹*Lancaster University, Lancaster LA1 4YB, United Kingdom*
⁹²*Imperial College London, London SW7 2AZ, United Kingdom*
⁹³*The University of Manchester, Manchester M13 9PL, United Kingdom*
⁹⁴*University of Arizona, Tucson, Arizona 85721, USA*
⁹⁵*University of California Riverside, Riverside, California 92521, USA*
⁹⁶*Florida State University, Tallahassee, Florida 32306, USA*
⁹⁷*University of Illinois at Chicago, Chicago, Illinois 60607, USA*
⁹⁸*Northern Illinois University, DeKalb, Illinois 60115, USA*
⁹⁹*Northwestern University, Evanston, Illinois 60208, USA*
¹⁰⁰*Indiana University, Bloomington, Indiana 47405, USA*
¹⁰¹*Purdue University Calumet, Hammond, Indiana 46323, USA*
¹⁰²*University of Notre Dame, Notre Dame, Indiana 46556, USA*
¹⁰³*Iowa State University, Ames, Iowa 50011, USA*
¹⁰⁴*University of Kansas, Lawrence, Kansas 66045, USA*
¹⁰⁵*Louisiana Tech University, Ruston, Louisiana 71272, USA*
¹⁰⁶*Northeastern University, Boston, Massachusetts 02115, USA*
¹⁰⁷*University of Mississippi, University, Mississippi 38677, USA*
¹⁰⁸*University of Nebraska, Lincoln, Nebraska 68588, USA*
¹⁰⁹*Rutgers University, Piscataway, New Jersey 08855, USA*
¹¹⁰*Princeton University, Princeton, New Jersey 08544, USA*
¹¹¹*State University of New York, Buffalo, New York 14260, USA*
¹¹²*State University of New York, Stony Brook, New York 11794, USA*
¹¹³*Brookhaven National Laboratory, Upton, New York 11973, USA*
¹¹⁴*Langston University, Langston, Oklahoma 73050, USA*
¹¹⁵*University of Oklahoma, Norman, Oklahoma 73019, USA*
¹¹⁶*Oklahoma State University, Stillwater, Oklahoma 74078, USA*
¹¹⁷*Oregon State University, Corvallis, Oregon 97331, USA*
¹¹⁸*Brown University, Providence, Rhode Island 02912, USA*
¹¹⁹*University of Texas, Arlington, Texas 76019, USA*
¹²⁰*Southern Methodist University, Dallas, Texas 75275, USA*
¹²¹*Rice University, Houston, Texas 77005, USA*
¹²²*University of Virginia, Charlottesville, Virginia 22904, USA*
¹²³*University of Washington, Seattle, Washington 98195, USA*

(Dated: September 13, 2017)

The CDF and D0 experiments at the Fermilab Tevatron have measured the asymmetry between yields of forward- and backward-produced top and antitop quarks based on their rapidity difference and the asymmetry between their decay leptons. These measurements use the full data sets collected in proton-antiproton collisions at a center-of-mass energy of $\sqrt{s} = 1.96$ TeV. We report the results of combinations of the inclusive asymmetries and their differential dependencies on relevant kinematic quantities. The combined inclusive asymmetry is $A_{\text{FB}}^{t\bar{t}} = 0.128 \pm 0.025$. The combined inclusive and differential asymmetries are consistent with recent standard model predictions.

PACS numbers: 14.65.Ha, 12.38.Qk, 11.30.Er, 13.85.-t

The production of top and antitop quark ($t\bar{t}$) pairs at the Tevatron proton-antiproton ($p\bar{p}$) collider at Fermilab is dominated by the $q\bar{q}$ annihilation process, which can lead to asymmetries, $A_{\text{FB}}^{t\bar{t}}$, in the number of top quarks produced within the hemisphere centered on the beam proton (forward) relative to those that are produced within the antiproton hemisphere (backward). In the standard model (SM), no forward-backward asymmetries are expected at leading order in perturbative quantum chromodynamics (QCD). However, contributions to the asymmetry from interference of leading order and

higher-order amplitudes, and smaller offsetting contributions from the interference of initial- and final-state radiation, combine to yield a non-zero asymmetry [1–5]. Compared to older predictions [6] of the inclusive asymmetry at next-to-leading order (NLO) QCD, the latest higher-order corrections in QCD and electroweak theory (EW) are almost of the same size as the inclusive prediction at NLO QCD. Measurements of the inclusive asymmetries and their dependence on kinematic quantities of top quarks and their decay leptons are used to probe the production mechanism. Beyond-the-SM (BSM) interac-

tions [7] can significantly alter the dynamics, even such that differential asymmetries can be strikingly changed while inclusive asymmetries are only marginally affected.

Inclusive and differential measurements [8, 9] by the CDF [10] and D0 [11] Collaborations in 2011 were only marginally consistent with each other, and with then-existing SM predictions [6]. Both collaborations have since completed measurements using the full Tevatron Run II $p\bar{p}$ collision data, corresponding to integrated luminosities between 9 and 10 fb^{-1} . Assuming SM t and \bar{t} decays, they have measured asymmetries using events containing a single charged lepton ($\ell+\text{jets}$), where one W boson from a top quark decays to a charged lepton and a neutrino and the other decays to a quark and an antiquark that evolve into jets, and in events containing two charged leptons ($\ell\ell$) where both W bosons decay leptonically. Both collaborations have measured inclusive and differential asymmetries as functions of kinematic quantities of the top quarks and their decay leptons. More refined analysis techniques have been employed since the initial measurements. In the $\ell+\text{jets}$ channel, CDF performed a detailed investigation of the inclusive and differential $t\bar{t}$ asymmetries [12], and D0 used a novel partial event reconstruction for the inclusive and differential measurement of $A_{\text{FB}}^{t\bar{t}}$ [13]. In the $\ell\ell$ channel, CDF used several kinematic distributions to minimize the expected total uncertainty [14], while D0 carried out a simultaneous measurement of $A_{\text{FB}}^{t\bar{t}}$ and the top quark polarization [15].

We present the combinations of the final CDF and D0 measurements and compare them with current SM calculations [16]. Careful assessment of the correlations of systematic uncertainties between analysis channels and experiments is required for comparing the data with predictions.

For reconstructed top and antitop quarks, $A_{\text{FB}}^{t\bar{t}}$ is defined by

$$A_{\text{FB}}^{t\bar{t}} = \frac{N(\Delta y_{t\bar{t}} > 0) - N(\Delta y_{t\bar{t}} < 0)}{N(\Delta y_{t\bar{t}} > 0) + N(\Delta y_{t\bar{t}} < 0)} , \quad (1)$$

where $\Delta y_{t\bar{t}} = y_t - y_{\bar{t}}$ is the rapidity difference [17] between the t and \bar{t} quark, and N is the signal yield in a particular configuration. Typically, measurements of $t\bar{t}$ forward-backward asymmetries require reconstruction of top and antitop quarks using all available information associated with the final-state particles [18]. Background contributions are subtracted from the yield of $t\bar{t}$ candidates, thereby providing the $t\bar{t}$ signal. The latter is corrected for detector effects, so as to unfold from the reconstructed t and \bar{t} quarks to the parton level.

The asymmetry in t and \bar{t} quark production also leads to asymmetries in their decay leptons which, while smaller in magnitude, do not need unfolding, but must be corrected for acceptance effects. The single-lepton asym-

metry is defined by

$$A_{\text{FB}}^{\ell} = \frac{N(q_{\ell}\eta_{\ell} > 0) - N(q_{\ell}\eta_{\ell} < 0)}{N(q_{\ell}\eta_{\ell} > 0) + N(q_{\ell}\eta_{\ell} < 0)} , \quad (2)$$

where q_{ℓ} is the sign of the electric charge and η_{ℓ} the pseudorapidity of the lepton in the laboratory frame. For the $\ell\ell$ channel, the dilepton asymmetry is defined as

$$A_{\text{FB}}^{\ell\ell} = \frac{N(\Delta\eta > 0) - N(\Delta\eta < 0)}{N(\Delta\eta > 0) + N(\Delta\eta < 0)} , \quad (3)$$

where $\Delta\eta = \eta_{\ell+} - \eta_{\ell-}$ is the pseudorapidity difference between the positive- and negative-charge lepton. The asymmetries obtained using top quarks and leptons are correlated, as a positive rapidity difference between a t and a \bar{t} quark is likely to produce a positive pseudorapidity difference between a positive- and negative-charge decay lepton.

Inclusive and differential measurements of $A_{\text{FB}}^{t\bar{t}}$ at the Tevatron were reported in Refs. [12, 13] for the $\ell+\text{jets}$ channel and in Refs. [14, 15] for the $\ell\ell$ channel. Measurements of A_{FB}^{ℓ} for the $\ell+\text{jets}$ channel are given in Refs. [19, 20] and in Refs. [21, 22] for the $\ell\ell$ channel. Measurements of $A_{\text{FB}}^{\ell\ell}$ are reported in Refs. [21, 22].

We combine the following CDF and D0 results using the best linear unbiased estimator (BLUE) [23–25]: the inclusive asymmetries $A_{\text{FB}}^{t\bar{t}}$, A_{FB}^{ℓ} , and $A_{\text{FB}}^{\ell\ell}$, each extrapolated to the full phase space relying on corresponding Monte Carlo simulations, and the differential asymmetry of $A_{\text{FB}}^{t\bar{t}}$ as a function of the invariant mass of the $t\bar{t}$ system ($m_{t\bar{t}}$). For combinations of inclusive asymmetries the input uncertainties are symmetrized, while they are treated as asymmetric in the case of the combination of the asymmetry as a function of $m_{t\bar{t}}$. A mutually compatible classification of all systematic uncertainties is not available for $A_{\text{FB}}^{t\bar{t}}$ as a function of $|\Delta y_{t\bar{t}}|$. Hence, we provide results of a simultaneous least-squares fit to determine the slope parameter of the asymmetry in the CDF and D0 data, assuming a linear dependence. A similar fit is also provided for $A_{\text{FB}}^{t\bar{t}}$ as a function of $m_{t\bar{t}}$. The CDF and D0 differential asymmetries, A_{FB}^{ℓ} as a function of $q_{\ell}\eta_{\ell}$ and $A_{\text{FB}}^{\ell\ell}$ as a function of $\Delta\eta$ are not combined, but are displayed together for ease of comparison.

Predictions of inclusive and differential $A_{\text{FB}}^{t\bar{t}}$ distributions at next-to-next-to-leading order (NNLO) QCD calculations are available from Ref. [1]. The contribution from EW NLO corrections to the NLO QCD asymmetries are not negligible [3]. Hence, we compare the measurements to the latest NNLO QCD + NLO EW inclusive and differential $A_{\text{FB}}^{t\bar{t}}$ calculations [1, 26]. The combined inclusive-lepton asymmetries A_{FB}^{ℓ} and $A_{\text{FB}}^{\ell\ell}$ are compared to the NLO QCD + NLO EW predictions of Ref. [3].

To accommodate correlations among analysis channels and between experiments, we classify systematic uncertainties into the following categories:

- (i) *Background modeling*: The uncertainties in the distribution and normalization of the background are

assumed to be uncorrelated since the backgrounds are estimated differently in different analyses, and in the two experiments.

- (ii) *Signal modeling:* The uncertainties in modeling the signal, parton showering [27], initial- and final-state radiation [28], and color connections [29] are taken to be fully correlated among analysis channels and experiments because they all rely on the same assumptions.
- (iii) *Detector modeling:* The uncertainties in jet-energy scale [30] and the modeling of the detector are fully correlated within each experiment and uncorrelated between the two experiments.
- (iv) *Method:* The uncertainties in the methods used to correct for detector acceptance, efficiency, and potential biases in the reconstruction of top quark kinematic properties are mostly taken to be uncorrelated between experiments and analysis channels. However, the uncertainties on the phase-space correction procedures for the leptonic asymmetry in the D0 $\ell + \text{jets}$ [13] and $\ell\ell$ [15] analyses are estimated using the same methods and are therefore correlated with each other but are uncorrelated with the CDF results.
- (v) *PDF:* The uncertainties in parton-density distribution functions (PDF) and the pileup in energy from overlapping $p\bar{p}$ interactions are treated as fully correlated between the analysis channels and the two experiments, because they characterize the same potential systematic biases.

The combined inclusive asymmetry is $A_{\text{FB}}^{t\bar{t}} = 0.128 \pm 0.021(\text{stat}) \pm 0.014(\text{syst})$, consistent with the NNLO QCD + NLO EW prediction of 0.095 ± 0.007 [2] within 1.3 standard deviations (SD). The combination has a χ^2 of 1.7 for 3 degrees of freedom (dof). BLUE also provides the weights in the combination for the CDF $\ell + \text{jets}$, D0 $\ell + \text{jets}$, CDF $\ell\ell$, and D0 $\ell\ell$ results, which are 0.25, 0.64, 0.01, and 0.11, respectively.

The CDF and D0 differential $A_{\text{FB}}^{t\bar{t}}$ asymmetries as a function of $m_{t\bar{t}}$ are measured only for the $\ell + \text{jets}$ channel. We combine the D0 bins in the range of $350 < m_{t\bar{t}} < 550$ GeV/c^2 to provide uniform, 100 GeV/c^2 -wide, bins for the combination. For the two measurements we use covariance matrices [31] that take into account the bin-to-bin correlations from the unfolding of differential distributions. The correlations in systematic uncertainties among channels and experiments for each $m_{t\bar{t}}$ bin are assumed to be equal to those in the inclusive measurements. However, the uncorrelated background uncertainties for the differential asymmetries are subdivided into two separate components, one for the overall normalization and one for the differential distribution (shape) of the background. According to the different experimental

methodologies, these are treated as correlated between bins for the CDF measurement and as uncorrelated for the D0 measurement. We verify that changing the correlations of systematic uncertainties between -1 and $+1$ has negligible impact on the combined result because the statistical uncertainties dominate.

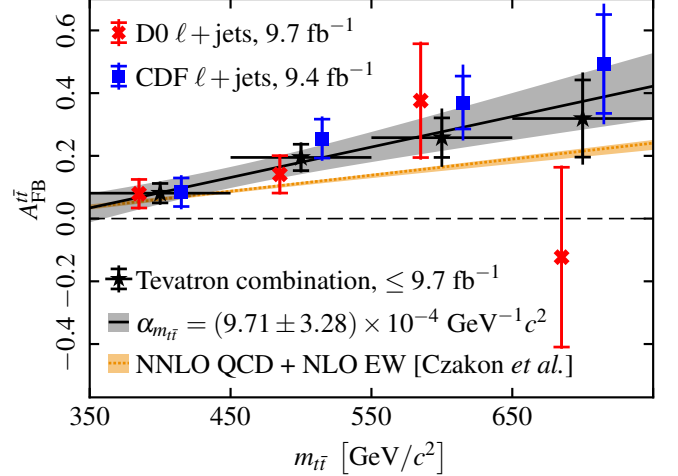


Figure 1. Results for $A_{\text{FB}}^{t\bar{t}}$ vs. $m_{t\bar{t}}$ for the individual CDF and D0 measurements and for their combination. The inputs to the combination are displaced at different abscissa values within each $m_{t\bar{t}}$ bin for ease of visibility. The inner error bar indicates the statistical uncertainty, while the outer error bar corresponds to the total uncertainty including the systematic uncertainty added in quadrature. The value of the combined data point for the mass region of $550 - 650$ GeV/c^2 is discussed in Ref. [31] in more detail. The linear dependence of the combined result is given by the solid black line together with the 1 SD total uncertainty of the two-parameter fit given by the shaded gray area. The dashed orange line shows the NNLO QCD + NLO EW prediction of Refs. [1, 2, 26], while the shaded orange area reflects its 1 SD uncertainty.

The combined $A_{\text{FB}}^{t\bar{t}}$ values, and their statistical and systematic uncertainties for each category, are given in Table I, which also reports the probabilities for the CDF and D0 inputs to agree with each other in each mass bin. Overall, the differential combination has a χ^2 of 5.2 for 4 dof. The correlations in the total uncertainties between $m_{t\bar{t}}$ bins are given in Ref. [31]. The values of $A_{\text{FB}}^{t\bar{t}}$ as a function of $m_{t\bar{t}}$ for each experiment and their combination are shown in Fig. 1, together with the NNLO QCD + NLO EW predictions [26].

The counter-intuitive value of the combined asymmetry in the $550 - 650$ GeV/c^2 mass bin is due to the specific pattern of the CDF and D0 bin-to-bin correlations stemming from different choices in the regularized matrix unfolding. The opposite correlations observed between the 600 GeV/c^2 and the 700 GeV/c^2 mass bins in the CDF (large and positive) and D0 (small and negative) measurements give rise to a combined asymmetry in the 600 GeV/c^2 bin that is smaller than that found in either

measurement [31].

To reduce the correlations between the slope and the intercept, we use a linear fit of the form $A_{\text{FB}}^{t\bar{t}}(m_{t\bar{t}}) = \alpha_{m_{t\bar{t}}}(m_{t\bar{t}} - 450 \text{ GeV}/c^2) + \beta_{m_{t\bar{t}}}$. The linear fit yields a slope of $\alpha_{m_{t\bar{t}}} = (9.71 \pm 3.28) \times 10^{-4} \text{ GeV}^{-1} c^2$ with an intercept at a $m_{t\bar{t}}$ value of 450 GeV/c^2 of $\beta_{m_{t\bar{t}}} = 0.131 \pm 0.034$. The fit has a χ^2 of 0.3 for 2 dof. The values predicted at NNLO QCD + NLO EW are $\alpha_{m_{t\bar{t}}}^{\text{SM}} = (5.11_{-0.64}^{+0.42}) \times 10^{-4} \text{ GeV}^{-1} c^2$ and an intercept of $\beta_{m_{t\bar{t}}}^{\text{SM}} = 0.087_{-0.006}^{+0.005}$. The predicted dependence is determined by a linear fit to the binned prediction from Ref. [26]. The NNLO QCD + NLO EW predictions of the differential $A_{\text{FB}}^{t\bar{t}}$ and of the slope parameters agree with the combined experimental results to within 1.3 SD.

The differential $t\bar{t}$ asymmetry as a function of $|\Delta y_{t\bar{t}}|$ is available from CDF for both the $\ell+\text{jets}$ and $\ell\ell$ channels, and from D0 for the $\ell+\text{jets}$ channel. The choice of binning differs for these measurements. We perform a simultaneous least-squares fit to a linear function $A_{\text{FB}}^{t\bar{t}}(|\Delta y_{t\bar{t}}|) = \alpha_{\Delta y_{t\bar{t}}} |\Delta y_{t\bar{t}}|$ for all available measurements, employing a combined 10×10 covariance matrix \mathcal{C}_{ij} . We define $\chi^2(|\Delta y_{t\bar{t}}|) = \sum_{ij} [y_i - f_i(|\Delta y_{t\bar{t}}|)] \mathcal{C}_{ij}^{-1} [y_j - f_j(|\Delta y_{t\bar{t}}|)]$, with y_i and y_j representing the bin i and j of each of the three measurements, and $f_i(|\Delta y_{t\bar{t}}|)$ and $f_j(|\Delta y_{t\bar{t}}|)$ representing the expectations from a linear function. The definition of the asymmetry ensures that $A_{\text{FB}}^{t\bar{t}} = 0$ at $\Delta y_{t\bar{t}} = 0$. The correlations of the systematic uncertainties among analysis channels and experiments are assumed to be equal to those in the $A_{\text{FB}}^{t\bar{t}}$ vs. $m_{t\bar{t}}$ measurements. Figure 2 shows the individual measurements and the result of the linear fit. The linear dependence for the combination is measured to be $\alpha_{\Delta y_{t\bar{t}}} = 0.187 \pm 0.038$ with a χ^2 of 10.9 for 9 dof. A fit to the binned NNLO QCD + NLO EW predictions of Ref. [1, 2, 26] gives the slope $\alpha_{\Delta y_{t\bar{t}}}^{\text{SM}} = 0.129_{-0.012}^{+0.006}$. The prediction and the combined result differ by 1.5 SD.

The combined fit to the CDF and D0 inclusive single-lepton asymmetries gives $A_{\text{FB}}^\ell = 0.073 \pm 0.016(\text{stat}) \pm 0.012(\text{syst})$. The fit has a χ^2 of 2.2 for 3 dof, and the result is consistent with the NLO QCD + NLO EW prediction of 0.038 ± 0.003 [3] to within 1.6 SD. The weights of the CDF $\ell+\text{jets}$, D0 $\ell+\text{jets}$, CDF $\ell\ell$ and D0 $\ell\ell$ results in the fit are 0.40, 0.27, 0.11, and 0.23, respectively. The individual CDF and D0 measurements of A_{FB}^ℓ as a function of $|q\eta_\ell|$ are shown in Fig. 3.

The combined fit to the CDF and D0 inclusive $A_{\text{FB}}^{\ell\ell}$ measurements yields $A_{\text{FB}}^{\ell\ell} = 0.108 \pm 0.043(\text{stat}) \pm 0.016(\text{syst})$. The fit has a χ^2 of 0.2 for 1 dof, and the result is consistent with the NLO QCD + NLO EW prediction of 0.048 ± 0.004 [3] to within 1.3 SD. The weights of the CDF and D0 $\ell\ell$ results in the fit are 0.32 and 0.68, respectively. The individual CDF and D0 measurements of $A_{\text{FB}}^{\ell\ell}$ as a function of $\Delta\eta$ are shown in Fig. 4.

In summary, we report combinations of the measurements of top-antitop quark forward-backward asymme-

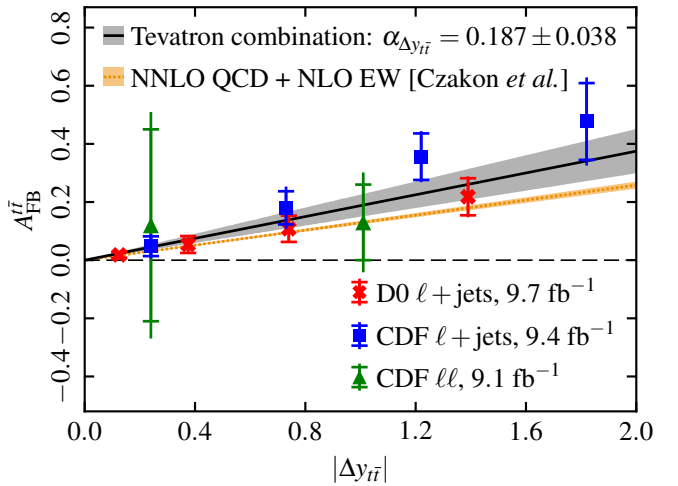


Figure 2. Measurements of the differential asymmetries $A_{\text{FB}}^{t\bar{t}}$ vs. $|\Delta y_{t\bar{t}}|$ with data points displayed at the distribution-weighted center of the bins. The inner error bar indicates the statistical uncertainty, while the outer error bar corresponds to the total uncertainty, including the systematic uncertainty added in quadrature. The combined linear dependence for all the experimental results is given by the solid black line, with the 1 SD total uncertainty on the one-parameter fit given by the shaded gray area. The dashed orange line shows the NNLO QCD + NLO EW prediction [1, 2, 26], while the shaded orange area reflects its 1 SD uncertainty.

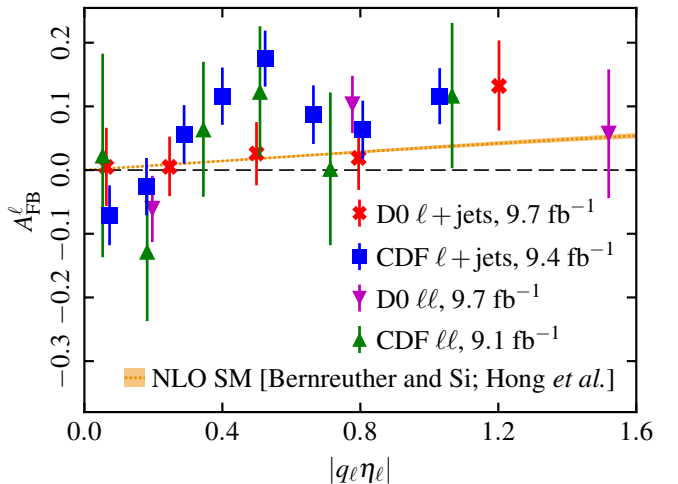


Figure 3. Comparison of the differential asymmetries A_{FB}^ℓ as a function of $|q\eta_\ell|$. Each error bar represents the total experimental uncertainty. The dashed orange line shows the NLO SM prediction [3, 32], while the shaded orange area shows its 1 SD uncertainty.

tries performed in a $p\bar{p}$ collision sample corresponding to $9-10 \text{ fb}^{-1}$ collected by the CDF and D0 experiments at the Tevatron. Both the inclusive and differential measurements favor somewhat larger positive asymmetries than the predictions. The resulting combined inclusive asymmetry is $A_{\text{FB}}^{t\bar{t}} = 0.128 \pm 0.025$ compared to the pre-

Table I. Combined differential $A_{FB}^{t\bar{t}}$ values in bins of $m_{t\bar{t}}$, with the probability (Prob) for the CDF and D0 inputs to agree with each other, with statistical (Stat), systematic (Tot syst), and total uncertainties. The systematic uncertainties are broken down into uncertainties in the distribution of the background (Bkd distr), background normalization (Bkd norm), signal modeling (Signal), detector modeling (Det), measurement method (Meth), and parton distribution function (PDF).

$m_{t\bar{t}}$ (GeV/ c^2)	$A_{FB}^{t\bar{t}}$	Prob	Uncertainty								
			Total	Stat	Meth	Signal	PDF	Det	Bkd distr	Bkd norm	Tot syst
350–450	0.081	95%	0.037	0.031	0.009	0.012	0.004	0.007	0.010	0.003	0.020
450–550	0.195	22%	0.048	0.042	0.010	0.016	0.007	0.006	0.007	0.006	0.023
550–650	0.258	98%	0.093	0.063	0.008	0.062	0.017	0.017	0.006	0.008	0.068
> 650	0.319	8%	0.147	0.123	0.018	0.065	0.021	0.026	0.019	0.019	0.080

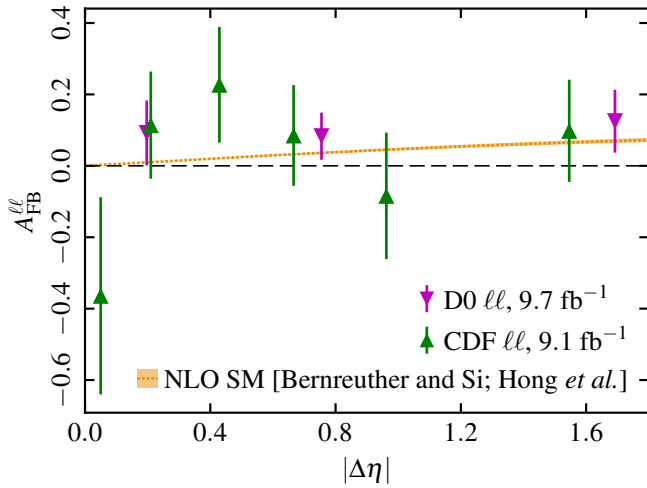


Figure 4. Comparison of the differential asymmetries $A_{FB}^{\ell\ell}$ as a function of $|\Delta\eta|$. Each error bar represents the total experimental uncertainty. The dashed orange line shows the NLO SM prediction [3, 32], while the shaded orange area shows its 1 SD uncertainty.

diction at NNLO QCD + NLO EW of 0.095 ± 0.007 . All three inclusive observables agree with the existing SM predictions to within 1.6 standard deviations. The differential asymmetries as a function of $m_{t\bar{t}}$ and $\Delta y_{t\bar{t}}$ agree to within 1.5 standard deviations. We conclude that the measurements and their combinations, shown in Fig. 5, are consistent with each other and with the SM predictions. The reported consistency is the result of an intense effort of refining the experimental and theoretical understanding, which started in 2010, when significant departures of the first Tevatron measurements [8, 9] from the predictions suggested potential contributions from BSM dynamics.

This document was prepared by the CDF and D0 collaborations using the resources of the Fermi National Accelerator Laboratory (Fermilab), a U.S. Department of Energy, Office of Science, HEP User Facility. Fermilab is managed by Fermi Research Alliance, LLC (FRA), acting under Contract No. DE-AC02-07CH11359.

We thank the staffs at Fermilab and collaborating institutions, and acknowledge support from the Department of Energy and the National Science Foundation (U.S.A.), the Australian Research Council (Australia), the National Council for the Development of Science and Technology and the Carlos Chagas Filho Foundation for the Support of Research in the State of Rio de Janeiro (Brazil), the Natural Sciences and Engineering Research Council (Canada), the China Academy of Sciences, the National Natural Science Foundation of China, and the National Science Council of the Republic of China (China), the Administrative Department of Science, Technology and Innovation (Colombia), the Ministry of Education, Youth and Sports (Czech Republic), the Academy of Finland, the Alternative Energies and Atomic Energy Commission and the National Center for Scientific Research/National Institute of Nuclear and Particle Physics (France), the Bundesministerium für Bildung und Forschung (Federal Ministry of Education and Research) and the Deutsche Forschungsgemeinschaft (German Research Foundation) (Germany), the Department of Atomic Energy and Department of Science and Technology (India), the Science Foundation Ireland (Ireland), the National Institute for Nuclear Physics (Italy), the Ministry of Education, Culture, Sports, Science and Technology (Japan), the Korean World Class University Program and the National Research Foundation of Korea (Korea), the National Council of Science and Technology (Mexico), the Foundation for Fundamental Research on Matter (Netherlands), the Ministry of Education and Science of the Russian Federation, the National Research Center Kurchatov Institute of the Russian Federation, and the Russian Foundation for Basic Research (Russia), the Slovak R&D Agency (Slovakia), the Ministry of Science and Innovation, and the Consolider-Ingenio 2010 Program (Spain), the Swedish Research Council (Sweden), the Swiss National Science Foundation (Switzerland), the Ministry of Education and Science of Ukraine (Ukraine), the Science and Technology Facilities Council and The Royal Society (United Kingdom), the A. P. Sloan Foundation (U.S.A.), and the European Union

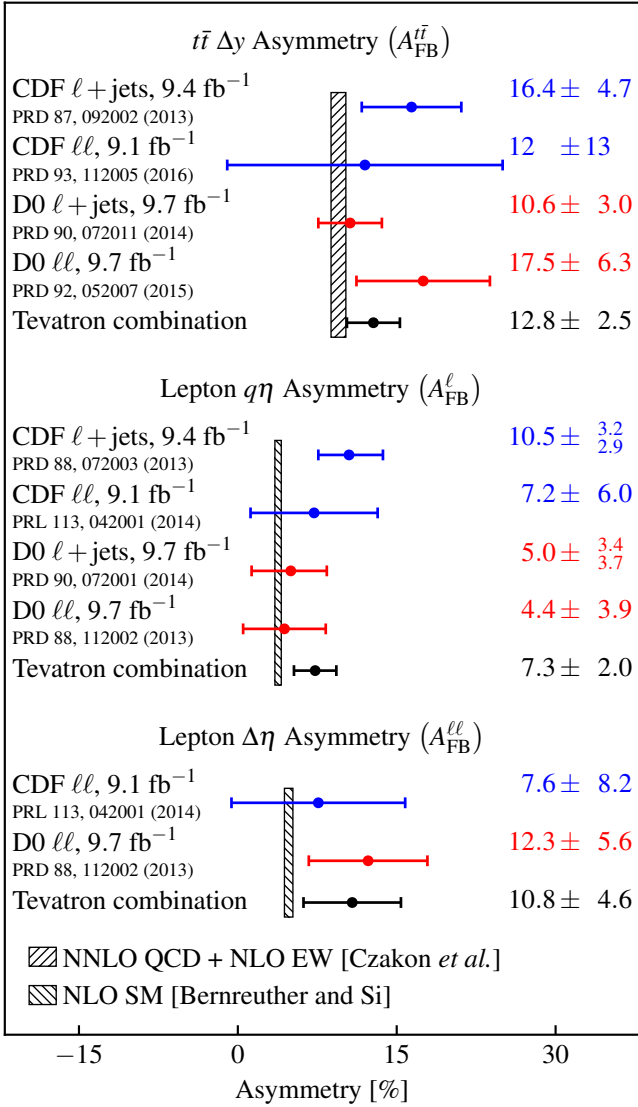


Figure 5. Summary of inclusive forward-backward asymmetries in $t\bar{t}$ events in percents at the Tevatron.

community Marie Curie Fellowship Contract No. 302103.

* Deceased

† With visitors from ^aUniversity of British Columbia, Vancouver, BC V6T 1Z1, Canada, ^bIstituto Nazionale di Fisica Nucleare, Sezione di Cagliari, 09042 Monserrato (Cagliari), Italy, ^cUniversity of California Irvine, Irvine, CA 92697, USA, ^dInstitute of Physics, Academy of Sciences of the Czech Republic, 182 21, Czech Republic, ^eCERN, CH-1211 Geneva, Switzerland, ^fCornell University, Ithaca, NY 14853, USA, ^gUniversity of Cyprus, Nicosia CY-1678, Cyprus, ^hOffice of Science, U.S. Department of Energy, Washington, DC 20585, USA, ⁱUniversity College Dublin, Dublin 4, Ireland, ^jETH, 8092 Zürich, Switzerland, ^kUniversity of Fukui, Fukui

City, Fukui Prefecture, Japan 910-0017, ^lUniversidad Iberoamericana, Lomas de Santa Fe, México, C.P. 01219, Distrito Federal, ^mUniversity of Iowa, Iowa City, IA 52242, USA, ⁿKinki University, Higashi-Osaka City, Japan 577-8502, ^oKansas State University, Manhattan, KS 66506, USA, ^pBrookhaven National Laboratory, Upton, NY 11973, USA, ^qIstituto Nazionale di Fisica Nucleare, Sezione di Lecce, Via Arnesano, I-73100 Lecce, Italy, ^rQueen Mary, University of London, London, E1 4NS, United Kingdom, ^sUniversity of Melbourne, Victoria 3010, Australia, ^tMuons, Inc., Batavia, IL 60510, USA, ^uNagasaki Institute of Applied Science, Nagasaki 851-0193, Japan, ^vNational Research Nuclear University, Moscow 115409, Russia, ^wNorthwestern University, Evanston, IL 60208, USA, ^xUniversity of Notre Dame, Notre Dame, IN 46556, USA, ^yUniversidad de Oviedo, E-33007 Oviedo, Spain, ^zCNRS-IN2P3, Paris, F-75205 France, ^{aa}Universidad Tecnica Federico Santa Maria, 110v Valparaiso, Chile, ^{bb}Sejong University, Seoul 143-747, Korea, ^{cc}The University of Jordan, Amman 11942, Jordan, ^{dd}Universite catholique de Louvain, 1348 Louvain-La-Neuve, Belgium, ^{ee}University of Zürich, 8006 Zürich, Switzerland, ^{ff}Massachusetts General Hospital, Boston, MA 02114 USA, ^{gg}Harvard Medical School, Boston, MA 02114 USA, ^{hh}Hampton University, Hampton, VA 23668, USA, ⁱⁱLos Alamos National Laboratory, Los Alamos, NM 87544, USA, ^{jj}Università degli Studi di Napoli Federico II, I-80138 Napoli, Italy

‡ With visitors from ^{kk}Augustana University, Sioux Falls, SD 57197, USA, ^{ll}The University of Liverpool, Liverpool L69 3BX, UK, ^{mm}Deutsches Elektronen-Synchrotron (DESY), Notkestrasse 85, Germany, ⁿⁿConsejo Nacional de Ciencia y Tecnología (Conacyt), M-03940 Mexico City, Mexico, ^{oo}SLAC, Menlo Park, CA 94025, USA, ^{pp}University College London, London WC1E 6BT, UK, ^{qq}Centro de Investigacion en Computacion - IPN, CP 07738 Mexico City, Mexico, ^{rr}Universidade Estadual Paulista, São Paulo, SP 01140, Brazil, ^{ss}Karlsruher Institut für Technologie (KIT) - Steinbuch Centre for Computing (SCC), D-76128 Karlsruhe, Germany, ^{tt}Office of Science, U.S. Department of Energy, Washington, D.C. 20585, USA, ^{uu}American Association for the Advancement of Science, Washington, D.C. 20005, USA, ^{vv}National Academy of Science of Ukraine (NASU) - Kiev Institute for Nuclear Research (KINR), Kyiv 03680, Ukraine, ^{ww}University of Maryland, College Park, MD 20742, USA, ^{xx}European Organization for Nuclear Research (CERN), CH-1211 Genève 23, Switzerland, ^{yy}Purdue University, West Lafayette, IN 47907, USA, ^{zz}Institute of Physics, Belgrade, CS-11080 Belgrade, Serbia

- [1] M. Czakon, P. Fiedler, D. Heymes, and A. Mitov, NNLO QCD predictions for fully-differential top-quark pair production at the Tevatron, *J. High Energy Phys.* **05** (2016) 034.
- [2] M. Czakon, P. Fiedler, and A. Mitov, Resolving the Tevatron Top Quark Forward-Backward Asymmetry Puzzle: Fully Differential Next-to-Next-to-Leading-Order Calculation, *Phys. Rev. Lett.* **115**, 052001 (2015).
- [3] W. Bernreuther and Z.-G. Si, Top quark and leptonic charge asymmetries for the Tevatron and LHC, *Phys. Rev. D* **86**, 034026 (2012).
- [4] N. Kidonakis, The top quark forward-backward asymmetry at approximate N^3LO , *Phys. Rev. D* **91**, 071502(R)

- (2015).
- [5] S.-Q. Wang, X.-G. Wu, Z.-G. Si, and S.J. Brodsky, Top-quark pair hadroproduction and a precise determination of the top-quark pole mass using the principle of maximum conformality, Subm. to J. High Energy Phys. SLAC-PUB-16934, [arXiv:1703.03583].
 - [6] S. Frixione and B.R. Webber, Matching NLO QCD computations and parton shower simulations, J. High Energy Phys. 06 (2002) 029; S. Frixione *et al.*, Matching NLO QCD and parton showers in heavy flavour production, J. High Energy Phys. 08 (2003) 007.
 - [7] J. F. Kamenik, J. Shu, and J. Zupan, Review of new physics effects in $t\bar{t}$ production, Eur. Phys. J. C **72**, 2102 (2012); See also Refs. 3–83 of E. L. Berger, Q.-H. Cao, C.-R. Chen and H. Zhang, Interpretations and implications of the top quark rapidity asymmetries $A_{\text{FB}}^{t\bar{t}}$ and A_{FB}^{ℓ} , Phys. Rev. D **88**, 014033 (2013).
 - [8] T. Aaltonen *et al.* (CDF Collaboration), Evidence for a mass dependent forward-backward asymmetry in top quark pair production, Phys. Rev. D **83**, 112003 (2011).
 - [9] V.M. Abazov *et al.* (D0 Collaboration), Forward-Backward Asymmetry in Top Quark-Antiquark Production, Phys. Rev. D **84**, 112005 (2011).
 - [10] D. Acosta *et al.* (CDF Collaboration), Measurement of the J/ψ meson and b -hadron production cross sections in $p\bar{p}$ collisions at $\sqrt{s} = 1960$ GeV, Phys. Rev. D **71**, 032001 (2005).
 - [11] V.M. Abazov *et al.* (D0 Collaboration), The Upgraded D0 Detector, Nucl. Instrum. Methods Phys. Res., Sect. A **565**, 463 (2006).
 - [12] T. Aaltonen *et al.* (CDF Collaboration), Measurement of the top quark forward-backward production asymmetry and its dependence on event kinematic properties, Phys. Rev. D **87**, 092002 (2013).
 - [13] V.M. Abazov *et al.* (D0 Collaboration), Measurement of the forward-backward asymmetry in top quark-antiquark production in $p\bar{p}$ collisions using the lepton+jets channel, Phys. Rev. D **90**, 072011 (2014).
 - [14] T. Aaltonen *et al.* (CDF Collaboration), Measurement of the forward-backward asymmetry of top-quark and antiquark pairs using the full CDF Run II data set, Phys. Rev. D **93**, 112005 (2016).
 - [15] V.M. Abazov *et al.* (D0 Collaboration), Simultaneous measurement of forward-backward asymmetry and top polarization in dilepton final states from $t\bar{t}$ production at the Tevatron, Phys. Rev. D **92**, 052007 (2015).
 - [16] J.A. Aguilar-Saavedra, D. Amidei, A. Juste, and M. Pérez-Victoria, Asymmetries in top quark pair production at hadron colliders, Rev. Mod. Phys. **87**, 421 (2015).
 - [17] The rapidity y is defined as $y(\theta, \beta) = 1/2 \cdot \ln[(1 + \beta \cdot \cos(\theta))/(1 - \beta \cdot \cos(\theta))]$, where θ is the polar angle relative to the proton beam and β is the ratio of a particle's momentum to its energy. The pseudo-rapidity is defined as $\eta = y(\theta, 1)$.
 - [18] B.A. Betchart, R. Demina, and A. Harel, Nucl. Instrum. Methods Phys. Res., Sect. A **736**, 169 (2014).
 - [19] T. Aaltonen *et al.* (CDF Collaboration), Measurement of the leptonic asymmetry in $t\bar{t}$ events produced in $p\bar{p}$ collisions at $\sqrt{s} = 1.96$ TeV, Phys. Rev. D **88**, 072003 (2013).
 - [20] V.M. Abazov *et al.* (D0 Collaboration), Measurement of the forward-backward asymmetry in the distribution of leptons in $t\bar{t}$ events in the lepton+jets channel, Phys. Rev. D **90**, 072001 (2014).
 - [21] V.M. Abazov *et al.* (D0 Collaboration), Measurement of the asymmetry in angular distributions of leptons produced in dilepton $t\bar{t}$ final states in $p\bar{p}$ collisions at $\sqrt{s} = 1.96$ TeV, Phys. Rev. D **88**, 112002 (2013).
 - [22] T. Aaltonen *et al.* (CDF Collaboration), Measurement of the Inclusive Leptonic Asymmetry in Top-Quark Pairs that Decay to Two Charged Leptons at CDF, Phys. Rev. Lett. **113**, 042001 (2014).
 - [23] L. Lyons, D. Gibaut, and P. Clifford, How to combine correlated estimates of a single physical quantity, Nucl. Instrum. Methods Phys. Res., Sect. A **270**, 110 (1988).
 - [24] L. Lyons, A.J. Martin, and D.H. Saxon, On the determination of the B lifetime by combining the results of different experiments, Phys. Rev. D **41**, 982 (1990).
 - [25] A. Valassi, Combining correlated measurements of several different physical quantities, Nucl. Instrum. Methods Phys. Res., Sect. A **500**, 391 (2003).
 - [26] M. Czakon, D. Heymes, A. Mitov, D. Pagani, I. Tsirnikos, and M. Zaro, Top-pair production at the LHC through NNLO QCD and NLO EW, [arXiv:1705.04105] (2017).
 - [27] G. Marchesini, B.R. Webber, G. Abbiendi, I.G. Knowles, M.H. Seymour, and L. Stanco, HERWIG: A Monte Carlo event generator for simulating hadron emission reactions with interfering gluons. Version 5.1 - April 1991, Comput. Phys. Commun. **67**, 465 (1992).
 - [28] B. Cooper, J. Katzy, M.L. Mangano, A. Messina, L. Mijovic, and P. Skands, Importance of a consistent choice of α_s in the matching of AlpGen and Pythia, Eur. Phys. J. C **72**, 2078 (2012).
 - [29] P.Z. Skands and D. Wicke, Non-perturbative QCD effects and the top mass at the Tevatron, Eur. Phys. J. C **52**, 133 (2007).
 - [30] V.M. Abazov *et al.* (D0 Collaboration), Jet energy scale determination in the D0 experiment, Nucl. Instrum. Methods Phys. Res., Sect. A **763**, 442 (2014),
 - [31] See Supplemental Material in the appendix for tables and figures with detailed uncertainty breakdown and additional information.
 - [32] Z. Hong, R. Edgar, S. Henry, D. Toback, Jonathan S. Wilson, and D. Amidei, Forward-backward asymmetry of leptonic decays of $t\bar{t}$ at the Fermilab Tevatron, Phys. Rev. D **90**, 014040 (2014).

Appendix: Supplemental material

In this appendix, we provide supplemental information on the combination of the CDF and D0 measurements of the forward-backward asymmetries in $t\bar{t}$ pair production at the Fermilab Tevatron.

$t\bar{t}$ production asymmetry, $A_{\text{FB}}^{t\bar{t}}$

Table II reports the uncertainties for each of the contributing measurements to the inclusive $t\bar{t}$ asymmetry, $A_{\text{FB}}^{t\bar{t}}$, and the uncertainties for their combination in the fit. Table III shows the individual inclusive $A_{\text{FB}}^{t\bar{t}}$ measurements and uncertainties, as well as their combination. The contribution, in terms of the weights determined by BLUE [23–25], of each measurement in the fit are also shown.

Table IV shows the inputs to the differential $A_{\text{FB}}^{t\bar{t}}$ vs. $m_{t\bar{t}}$ fit and their uncertainties. Figure 6 shows the combined result for the differential $A_{\text{FB}}^{t\bar{t}}$ vs. $m_{t\bar{t}}$ data. The linear fit to the data and its one standard deviation (SD) uncertainty are shown by the black solid line and gray shaded band; the corresponding quantities for the theoretical prediction are shown by the orange line and shaded band. Figure 7 shows the correlations of the slope and intercept at $m_{t\bar{t}} = 450$ GeV/c² for the data and theoretical prediction. The smaller orange ellipse shows the correlation of the slope and intercept of the NNLO QCD + NLO EW prediction of Ref. [1, 2, 26].

Figure 8 shows the correlations of total uncertainties between adjacent $m_{t\bar{t}}$ bins, for the CDF and D0 data, as well as for the combination. The correlations between the individual CDF and D0 measurements for the third bin with adjacent bins of $m_{t\bar{t}}$ result in a combined asymmetry value that is smaller than either of the inputs for the third bin. This behavior indicates the presence of large correlations and can be understood when looking at the orientation of the correlation ellipses in Figure 8(c). The 68% confidence level ellipses show smaller uncertainties for the CDF inputs than for the D0 inputs. The smaller CDF uncertainties results from the different choice made by CDF for the regularization method used to correct for detector effects.

Table V shows the covariance matrix of the combined differential $A_{\text{FB}}^{t\bar{t}}$ vs. $m_{t\bar{t}}$. Table VI shows the inputs to the differential $A_{\text{FB}}^{t\bar{t}}$ vs. $|\Delta y_{t\bar{t}}|$ fit and their uncertainties. Table VII shows the covariance matrix of total uncertainties of the differential $A_{\text{FB}}^{t\bar{t}}$ vs. $|\Delta y_{t\bar{t}}|$ inputs to the combined fit.

Single lepton asymmetry, A_{FB}^{ℓ}

Table VIII reports the uncertainties for each of the contributing measurements to the inclusive single lepton asymmetry, A_{FB}^{ℓ} , and the uncertainties for their combination in the fit. Table IX shows the individual inclusive A_{FB}^{ℓ} measurements and uncertainties, as well as their combination. The weights of each measurement in the fit are also shown.

Dilepton asymmetry, $A_{\text{FB}}^{\ell\ell}$

Table X reports the uncertainties for each of the contributing measurements to the inclusive dilepton asymmetry $A_{\text{FB}}^{\ell\ell}$ and the uncertainties for their combination in the fit. Table XI shows the individual inclusive $A_{\text{FB}}^{\ell\ell}$ measurements and uncertainties, as well as their combination. The weights of each measurement in the fit are also shown.

Table II. Statistical and systematic uncertainties in the individual inclusive $A_{\text{FB}}^{t\bar{t}}$ inputs as well as in the resultant combination.

Uncertainty	CDF $\ell+\text{jets}$ [12]	CDF $\ell\ell$ [14]	D0 $\ell+\text{jets}$ [13]	D0 $\ell\ell$ [15]	Combination
Statistical	0.039	0.11	0.027	0.056	0.021
Background	0.022	0.04	0.010	0.007	0.008
Signal	0.011	0.05	0.005	0.026	0.009
Detector	0.007	0.02	0.003	0.001	0.003
Method	0.004	0.02	0.005	0.014	0.004
PDF	0.001	0.01	0.004	0.003	0.003

Table III. Inputs to the combination of the inclusive $t\bar{t}$ asymmetries and results of the combination.

Analysis	$A_{\text{FB}}^{t\bar{t}}$	Uncertainty			Weight
		Stat.	Syst.	Total	
CDF $\ell+\text{jets}$ [12]	0.164	0.039	0.026	0.047	0.25
CDF $\ell\ell$ [14]	0.12	0.11	0.07	0.13	0.01
D0 $\ell+\text{jets}$ [13]	0.106	0.027	0.013	0.030	0.64
D0 $\ell\ell$ [15]	0.175	0.056	0.031	0.063	0.11
Combination	0.128	0.021	0.014	0.025	

Table IV. Inputs of the $A_{\text{FB}}^{t\bar{t}}$ results in the $\ell+\text{jets}$ channels, along with their statistical (Stat) and systematic uncertainties broken down for the individual $m_{t\bar{t}}$ bins. The listed systematic uncertainties originate from the measurement method (Method), signal modeling (Signal), parton-distribution function (PDF), detector modeling (Detector), and from background shape (Bkd dist) and background normalization (Bkd norm).

$m_{t\bar{t}}$ [GeV/ c^2]	$A_{\text{FB}}^{t\bar{t}}$	Uncertainty							
		Total	Stat	Method	Signal	PDF	Detector	Bkd dist	Bkd norm
<u>D0 $\ell+\text{jets}$</u>									
350–450	0.079	0.050	0.046	0.011	0.015	0.005	0.005	0.007	0.001
450–550	0.141	0.064	0.060	0.018	0.010	0.011	0.0024	0.007	0.001
550–650	0.376	0.188	0.181	0.011	0.028	0.035	0.018	0.010	0.002
> 650	-0.123	0.292	0.287	0.017	0.009	0.043	0.030	0.014	0.003
<u>CDF $\ell+\text{jets}$</u>									
350–450	0.084	0.055	0.046	0.012	0.009	0.001	0.013	0.021	0.008
450–550	0.255	0.071	0.062	0.002	0.021	0.001	0.013	0.017	0.016
550–650	0.370	0.121	0.084	0.001	0.077	0.001	0.032	0.011	0.021
> 650	0.493	0.193	0.158	0.023	0.091	0.001	0.045	0.021	0.031

Table V. Covariance matrix of the combined CDF and D0 differential $A_{\text{FB}}^{t\bar{t}}$ vs. $m_{t\bar{t}}$.

$m_{t\bar{t}}$ [GeV/ c^2]	350–450	450–550	550–650	> 650
350–450	+0.0013690	+0.0007672	+0.0002512	+0.0003644
450–550	+0.0007672	+0.0023040	+0.0012140	-0.0005292
550–650	+0.0002512	+0.0012140	+0.0086490	+0.0057140
> 650	+0.0003644	-0.0005292	+0.0057140	+0.0216100

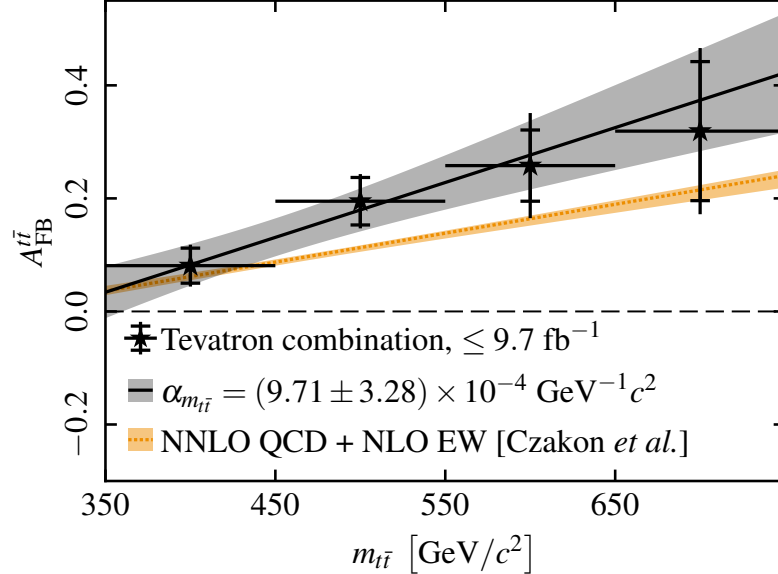


Figure 6. Differential $A_{FB}^{t\bar{t}}$ vs. $m_{t\bar{t}}$ for the Tevatron combination. The linear slope of the combined result is given by the solid black line together with the total uncertainty of the two-parameter fit (shaded gray area). The dashed solid orange line shows the NNLO QCD + NLO EW prediction of Refs. [1, 2, 26], while the shaded orange area shows the 1 SD theoretical uncertainty on the prediction.

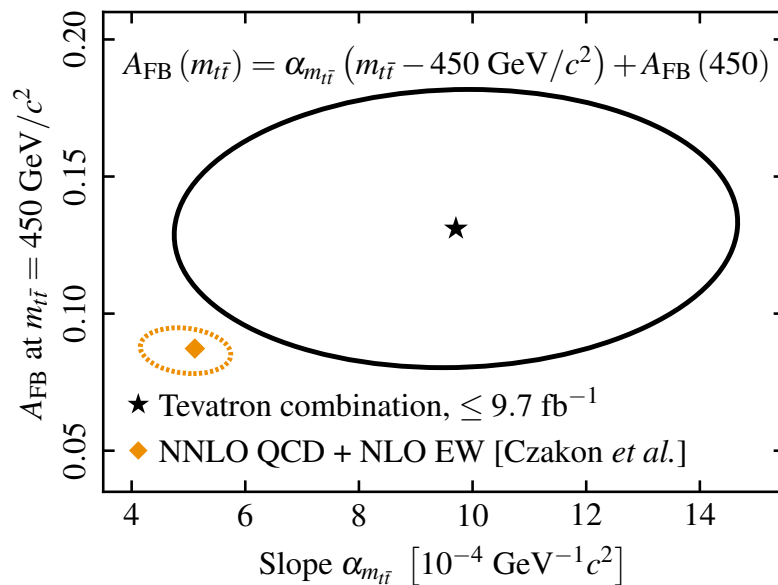


Figure 7. Correlation of the slope and intercept from the linear fit of the $A_{FB}^{t\bar{t}}$ vs. $m_{t\bar{t}}$ data represented as 68% confidence ellipses, and shown at $m_{t\bar{t}} = 450$ GeV/ c^2 . The smaller dashed orange ellipse shows the correlation of the slope and intercept of the NNLO QCD + NLO EW prediction of Refs. [1, 2, 26].

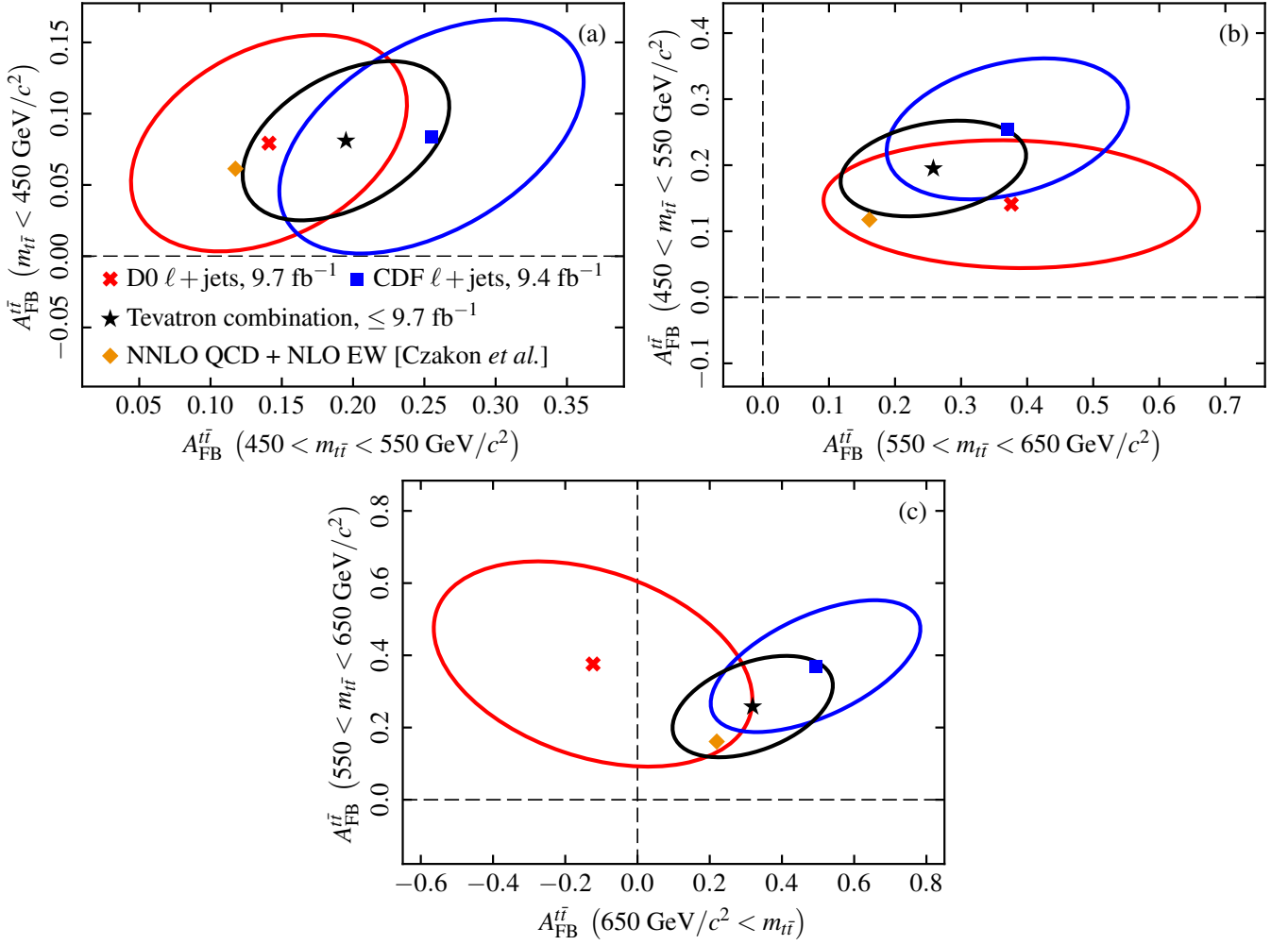


Figure 8. Correlations of combined statistical and systematic uncertainties represented as 68% confidence ellipses between the first and second $A_{\text{FB}}^{t\bar{t}}$ vs. $m_{t\bar{t}}$ bin (a), the second and third $A_{\text{FB}}^{t\bar{t}}$ vs. $m_{t\bar{t}}$ bin (b), and the third and fourth $A_{\text{FB}}^{t\bar{t}}$ vs. $m_{t\bar{t}}$ bin (c). The orange marker shows the NNLO QCD + NLO EW theoretical prediction [1, 2, 26] while the dashed orange ellipse shows the theoretical uncertainty on the prediction.

Table VI. Inputs of the differential $A_{\text{FB}}^{t\bar{t}}$ vs. $|\Delta y_{t\bar{t}}|$ results in the $\ell+\text{jets}$ channels and $\ell\ell$ channel. Their statistical and systematic uncertainties are broken down for the individual $|\Delta y_{t\bar{t}}|$ bins. The listed systematic uncertainties originate from the measurement method (Method), signal modeling (Signal), parton-distribution function (PDF), detector modeling (Detector), and from background shape (Bkd dist) and background normalization (Bkd norm).

$\Delta y_{t\bar{t}}$	$A_{\text{FB}}^{t\bar{t}}$	Uncertainty							
		Total	Statistical	Method	Signal	PDF	Detector	Bkd dist	Bkd norm
<u>D0 $\ell+\text{jets}$</u>									
0.00–0.25	0.018	0.012	0.010	0.004	0.004	0.002	0.003	0.004	0.001
0.25–0.50	0.054	0.033	0.029	0.009	0.008	0.003	0.005	0.008	0.001
0.50–1.00	0.108	0.048	0.045	0.010	0.009	0.004	0.006	0.009	0.001
> 1.00	0.218	0.071	0.064	0.017	0.015	0.007	0.010	0.016	0.002
<u>CDF $\ell+\text{jets}$</u>									
0.00–0.50	0.048	0.042	0.034	0.004	0.017	0.001	0.005	0.017	0.005
0.50–1.00	0.180	0.074	0.057	0.008	0.027	0.001	0.015	0.029	0.017
1.00–1.50	0.356	0.088	0.080	0.001	0.013	0.001	0.004	0.005	0.032
> 1.50	0.477	0.151	0.132	0.018	0.034	0.004	0.012	0.044	0.043
<u>CDF $\ell\ell$</u>									
0.00–0.50	0.12	0.39	0.33	0.06	0.16	0.01	0.02		0.13
> 0.50	0.13	0.17	0.13	0.02	0.09	0.01	0.02		0.06

Table VII. Covariance matrix of the statistical and systematic uncertainties of the differential $A_{\text{FB}}^{t\bar{t}}$ vs. $|\Delta y_{t\bar{t}}|$ results employed in the combined χ^2 fit. The PDF and signal uncertainties are assumed to be fully correlated between CDF and D0 (+1), while others are assumed to be uncorrelated.

$\Delta y_{t\bar{t}}$		D0 $\ell+\text{jets}$			CDF $\ell+\text{jets}$			CDF $\ell\ell$			
0.00-0.25	0.25-0.50	0.50-1.00	>1.00	0.00-0.50	0.50-1.00	>1.50	0.00-0.50	0.50-1.00	>1.50	0.00-0.50	>0.50
D0 $\ell+\text{jets}$											
0.00-0.25	+1.5590e-04	+3.1260e-04	+4.3580e-04	+2.0598e-04	+6.7363e-05	+1.0965e-04	+5.4530e-05	+1.4314e-04	+6.1059e-04	+3.8000e-04	
0.25-0.50	+3.1260e-04	+1.0914e-03	+1.3690e-03	+5.2010e-04	+1.3438e-04	+2.1827e-04	+1.0809e-04	+2.8259e-04	+1.2112e-03	+7.5000e-04	
0.50-1.00	+4.3580e-04	+1.3690e-03	+2.3518e-03	+1.1144e-03	+1.5107e-04	+2.4518e-04	+1.2126e-04	+3.1653e-04	+1.3588e-03	+8.4000e-04	
>1.00	+2.0598e-04	+5.2010e-04	+1.1144e-03	+4.9802e-03	+2.5234e-04	+4.1067e-04	+2.0392e-04	+5.3492e-04	+2.2847e-03	+1.4200e-03	
CDF $\ell+\text{jets}$											
0.00-0.50	+6.7363e-05	+1.3438e-04	+1.5107e-04	+2.5234e-04	+1.7632e-03	+2.0343e-03	+2.0723e-05	-2.0149e-03	+2.5367e-03	-1.3013e-03	
0.50-1.00	+1.0965e-04	+2.1827e-04	+2.4518e-04	+4.1067e-04	+2.0343e-03	+5.3518e-03	+2.4451e-03	-2.7678e-04	-1.4144e-04	+1.1556e-04	
1.00-1.50	+5.4530e-05	+1.0809e-04	+1.2126e-04	+2.0392e-04	+2.0723e-05	+2.4451e-03	+7.6970e-03	+1.1443e-02	-5.2223e-04	+6.4377e-04	
>1.50	1.4314e-04	+2.8259e-04	+3.1653e-04	+5.3492e-04	-2.0149e-03	-2.7678e-04	+1.1443e-02	+2.2995e-02	-3.0824e-03	+2.6086e-03	
CDF $\ell\ell$											
0.00-0.50	+6.1059e-04	+1.2112e-03	+1.3588e-03	+2.2847e-03	+2.5367e-03	-1.4144e-04	-5.2223e-04	-3.0824e-03	+1.5170e-01	-2.2280e-02	
>0.50	+3.8000e-04	+7.5000e-04	+8.4000e-04	+1.4200e-03	-1.3013e-03	+1.1556e-04	+6.4377e-04	+2.6086e-03	-2.2280e-02	+2.9500e-02	

Table VIII. Statistical and systematic uncertainties in the individual inclusive A_{FB}^{ℓ} inputs.

Uncertainty	CDF $\ell+\text{jets}$ [19]	CDF $\ell\ell$ [22]	D0 $\ell+\text{jets}$ [20]	D0 $\ell\ell$ [21]	Combination
Statistical	0.024	0.052	0.027	0.037	0.016
Background	0.015	0.029	$^{+0.016}_{-0.018}$	0.008	0.008
Signal	0.007	< 0.001	0.008	0.005	0.006
Detector	0.002	0.004	$^{+0.008}_{-0.011}$	0.005	0.004
Method	$^{+0.013}_{-0.000}$	0.006	0.008	0.004	0.005
PDF	0.003	< 0.001	0.002	< 0.001	0.002

Table IX. Inputs to and results from the combination of the inclusive A_{FB}^{ℓ} asymmetries.

Analysis	A_{FB}^{ℓ}	Uncertainty			Weight
		Stat.	Syst.	Total	
CDF $\ell+\text{jets}$ [19]	0.105	0.024	$^{+0.022}_{-0.017}$	$^{+0.032}_{-0.029}$	0.40
CDF $\ell\ell$ [22]	0.072	0.052	0.030	0.060	0.11
D0 $\ell+\text{jets}$ [20]	0.050	0.027	$^{+0.020}_{-0.024}$	$^{+0.034}_{-0.037}$	0.27
D0 $\ell\ell$ [21]	0.044	0.037	0.011	0.039	0.23
Combination	0.073	0.016	0.012	0.020	

Table X. Statistical and systematic uncertainties in the individual inclusive $A_{\text{FB}}^{\ell\ell}$ inputs as well as in the combined results.

Uncertainty	CDF $\ell\ell$ [22]	D0 $\ell\ell$ [21]	Combination
Statistical	0.072	0.054	0.043
Background	0.037	0.009	0.013
Signal	< 0.001	0.009	0.001
Detector	0.003	0.006	0.008
Method	0.013	0.004	0.005
PDF	< 0.001	< 0.001	0.001

Table XI. Inputs to and results from the combination of the inclusive $A_{\text{FB}}^{\ell\ell}$ asymmetries.

Analysis	$A_{\text{FB}}^{\ell\ell}$	Uncertainty			Weight
		Stat.	Syst.	Total	
CDF $\ell\ell$ [22]	0.076	0.072	0.037	0.082	0.32
D0 $\ell\ell$ [21]	0.123	0.054	0.015	0.056	0.68
Combination	0.108	0.043	0.016	0.046	